JOURNAL OF MATERIALS SCIENCE 32 (1997) 2381–2386

Piezoelectric behaviour of PZT doped with calcium: a combined experimental and theoretical study

M. CERQUEIRA, R. S. NASAR, E. LONGO
Laboratório Interdisciplinar de Eletroquímica e Cerâmica, Departamento de Química, UFSCar, Caixa Postal 676, 13565 São Carlos-SP, Brazil

J. A. VARELA
Instituto de Química, UNESP, Caixa Postal 355, 14800-900 Araraquara-SP, Brazil

A. BELTRÁN*, R. LLUSAR, J. ANDRÉS
Departament de Ciències Experimentals, Universitat Jaume I, Box 242, 12080 Castelló, Spain

An experimental and theoretical study on the piezoelectric behaviour of PZT doped with a range of calcium ion concentrations is presented. A systematic study of the effect on the piezoelectric properties of PZT doped with various concentrations of CaO at constant sintering temperature and sintering time was carried out. The remanent polarization, planar coupling factor and frequency–thickness constant increase with calcium concentration. *Ab initio* perturbed ion calculations show that the lattice energy decreases with calcium addition for both tetragonal and rhombohedral phases of PZT.

1. Introduction

$Pb(Zr,Ti)O_3$ (PZT) is a solid solution of lead zirconate and lead titanate that presents piezoelectric behaviour with important technological applications [1–7]. This perovskite structured material presents ferroelectric properties when its phase has a non-centrosymmetric structure, i.e. tetragonal, rhombohedral or orthorhombic, and they become paraelectric when the crystal structure transforms from tetragonal to cubic at the Curie temperature. In particular, ferroelectric properties are known to originate from displacive transitions [8] of Ti^{4+}/Zr^{4+} cations between two stable off-centred sites of TiO_6ZrO_6 octahedra, respectively, in response to an external field. The remanent polarization, P_r, and coercive field, E_c, are intimately related to deformation of the lattice [9]. The piezoelectric properties are dependent on the ratio of the starting materials, synthesis procedure, processing and doping methods [10–13]. However, the best piezoelectric properties of PZT (high dielectric constant, ε, and planar coupling factor, K_p) exist in the phase boundary between the tetragonal and rhombohedral phases, known as the morphotropic phase boundary (MPB) [14, 15].

There is a general agreement that the first step of the mixed-oxide reaction route for compositions near the MPB is the reaction of PbO with TiO_2 to form $PbTiO_3$ [16] and the accepted route to yield the formation of both $PbTiO_3$ and $PbZrO_3$ is the subsequent reaction to form PZT solid solution [16–19]. The presence was also reported of an intermediate tetragonal solid solution of PbO with a small amount of TiO_2 and a trace of ZrO_2 [20, 21]. In this sense, Kulcsar [22] and Bernard [23] have observed that the doping process of Sr^{2+} and Ca^{2+} in the Pb^{2+} position increase the K_p value. Recently, Zhang *et al.* [24], studying the piezoelectric response in the region of MPB, proved that below 300 K, the transformation of piezoelectric and dielectric properties are due to the change of activity of the wall domains in the material.

Structural investigations of PZT solid solutions found either a rhombohedral phase or a tetragonal phase at room temperature, depending on the composition ratio Zr/Ti, which are separated by MPB [25]. Substitutions of Zr^{4+} for Ti^{4+} in $PbTiO_3$ reduce the tetragonal distortion and ultimately cause the appearance of another ferroelectric phase of rhombohedral $R3m$ symmetry [26]. Still more Zr^{4+} causes the appearance of the orthorhombic antiferroelectric $PbZrO_3$ phase with some stability of a tetragonal antiferroelectric phase near the Curie point. In this sense, Jaffe *et al.* [9] consider that the tetragonal phase favours piezoelectric properties in opposition to the effect caused by the rhombohedral phase. Comes [27], however, proposed that the polarization is dependent on crystallographic direction, the tetragonal phase consists of displacements along four cube diagonals, giving an average structure with a polarization along [1 0 0] whilst the rhombohedral phase is ordered along [1 1 1].

In this study a combined experimental and theoretical approach to piezoelectric behaviour of PZT doped with Ca^{2+} is presented. In the experimental part, a systematic study of the variation of

* Author to whom correspondence should be addressed.

0022–2461

piezoelectric properties of PZT with CaO concentrations at constant temperature and sintering time is carried out. There have been recent achievements in applying *ab initio* perturbed ion (aiPI) methodology [28–30] in order to acquire an understanding of the physical and chemical properties relevant to condensed matter [31–35]. Following this method we have investigated, from a theoretical point of view, the following aspects: (i) the influence of the Ti^{4+}/Zr^{4+} displacement along the *c*-axis on the lattice energies of Ca^{2+}-doped (0.25–1.5 mol %) tetragonal and rhombohedral PZT structures, and (ii) the evolution of the ion–lattice interaction for each of the ions present in the lattice as a function of the calcium concentration. A comparison between our experimental and theoretical results is then carried out in order to understand the piezoelectric behaviour of PZT doped with calcium.

2. Experimental procedure

The purity and origin of the raw materials were as follows: $Pb(NO_3)_2$ (99.3%, Merck); ZrO_2 (99.6%, Merck); TiO_2 (99.2, Aldrich); $Ca(CH_3–CoO)_2$ (99.2%, Reagen). A composition of $(Zr_{0.53}Ti_{0.47})O_2$ powder (ZT) was prepared by mixing and grinding zirconia and titania powders for 24 h in isopropyl alcohol media. The powder was dried and then calcined at 1450 °C for 2 h. After calcination, the material was deagglomerated in alumina mortar and then characterized by X-ray diffraction (Siemens model D-5000).

The solid solution ZT was diluted in water whilst stirring. A stoichiometric amount of lead nitrate was dissolved in this solution. To precipitate $Pb(OH)_2$ on the ZT particles, NH_4OH was added to the solution until the pH reached the value of 11. The precipitate was washed, filtered and dried in oven at 60 °C.

Calcium acetate was diluted in isopropyl alcohol and mixed with the precipitates $ZT + Pb(OH)_2$. The solution was stirred for 2 h and then dried, deagglomerated in mortar and granulated in 200 mesh screen. The amount of calcium acetate was calculated to give concentrations of 0.25, 0.50, 1.0 and 1.5 mol % related to the precipitates.

This material was calcined at 850 °C for 2 h and the calcium-doped PZT phases analysed by the Rietveld method [36]. This method consists in a comparison of the calculated X-ray diffraction spectrum, obtained from defined crystallographic data, with the experimental X-ray diffraction spectrum. The approximation is made by the least squares method.

Surface areas measured in the calcium-doped PZT were determined by the nitrogen adsorption (model ASAP-2000 Micromeretics) and the value of $0.4\ m^2\ g^{-1}$ was found to be independent of the calcium concentration.

The powders were pressed into pellets 12 mm diameter and about 2 mm thick, by uniaxial pressing of 20 MPa followed by isostatic pressing with 200 MPa. All compositions were sintered at 1150 °C for 3 h and characterized by X-ray diffraction.

The PZT pellets with 0.25, 0.50, 1.0 and 1.5 mol % calcium were polished up to 1 mm thick. Platinum electrodes were applied to the samples surfaces by sputtering. Electric fields in the range of 1.0 to $3.5\ kV\ nm^{-1}$ were then applied to these samples for poling. The fundamental resonance frequencies were obtained by using a complex impedance meter (model HP 4194 by Hewlett Packard).

3. Theoretical methods and models

3.1. Method

The aiPI method provides an adequate quantum-mechanical treatment of the atom-in-the-lattice structure and has been presented by Luaña *et al.* [29, 30]; here we only summarize its main features.

According to the theory of electronic separability [37, 38], if a system can be partitioned into weakly interacting groups, its electronic wave function can be written as an antisymmetrized product of wave functions. If Ψ_A is the wave function of a particularly relevant group, i.e. the active (A) group, whose self-consistent field (SCF) equations are solved in the field of the remaining (frozen) groups. The contributions of the A group to the total energy can be collected in the effective energy

$$E^{A}_{eff} = E^{A}_{net} + \sum_{R(\neq A)} E^{AR}_{int} = E^{A}_{net} + E^{A}_{int} \qquad (1)$$

which, by minimization, gives the best Ψ_A for a set of given frozen groups.

The effective energy arises from the contribution of internal energy of the group, E_{net}, and the interaction energy, E_{int}, for this group with each of the ions in the lattice.

The total energy of the system is not the sum of the group effective energies. However, we can define the additive energy of the *A* group as

$$E^{A}_{add} = E^{A}_{net} + \tfrac{1}{2} E^{A}_{int} \qquad (2)$$

For an $A_aB_bC_c\ldots$ ionic crystal, the ions (A, B, C, …) are stabilized by ion-lattice interaction energy, and the crystal energy per molecule is

$$E_{cryst} = aE^{A}_{add} + bE^{B}_{add} + cE^{C}_{add} + \ldots = aE^{A}_{net} + bE^{B}_{net} + cE^{C}_{net} + \ldots + \tfrac{1}{2}(aE^{A}_{int} + bE^{B}_{int} + cE^{C}_{int} + \ldots) \qquad (3)$$

the lattice energy (E_{latt}) in the aiPI method is given by

$$E_{latt} = E_{cryst} - (aE^{A}_{0} + bE^{B}_{0} + cE^{C}_{0} + \ldots) \qquad (4)$$

where the subscript 0 stands for free-ion values.

3.2. Basis set representation

Large STO basis sets have been used on each atomic centre 7s5p on Ca^{2+} and Ti^{4+}, 5s5p on O^{2-}, 10s9p5d on Zr^{4+} [39] and 12s8p6d2f on Pb^{2+} [40]. The optimization of these basis sets was done in order to minimize the total energy while maintaining SCF stability. The quantum mechanical contributions to the interaction energies have been considered for a large number of neighbouring shells up to attaining a convergence of 10^{-6} Hartrees in the crystal energy. The crystal energy, on the other hand, includes correlation estimated by means of the unrelaxed

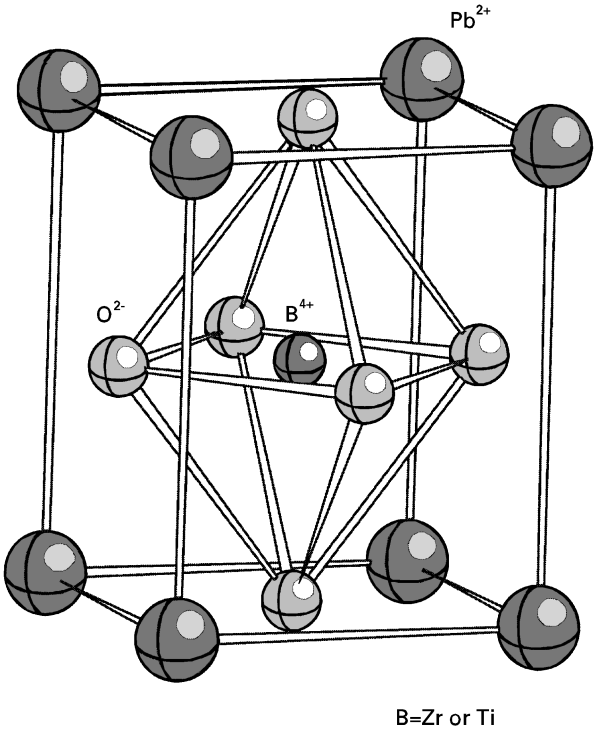

Figure 1 The PZT tetragonal structure.

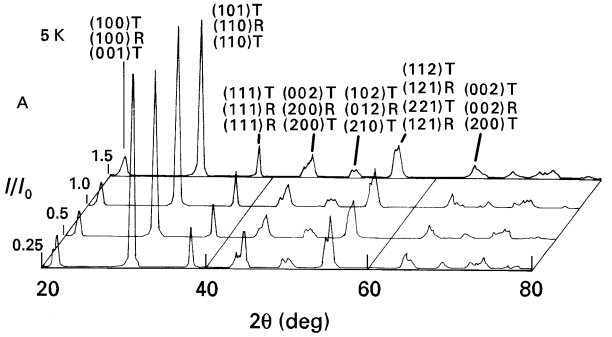

Figure 2 The X-ray diffraction pattern of the Ca-PZT samples.

TABLE I Relative density, ρ/ρ_T, planar coupling factor, K_p, frequency–thickness constant, N_p, and fraction of tetragonal phase, F_t, of pure 53/47 and calicium-doped PZT 53/47

	Dopant (%)	K_p	ρ/ρ_T (%)	N_p (Hz cm)	F_t (%)
Ca-PZT	0.25	0.48	96.0	2191	63
	0.50	0.52	98.4	2299	47
	1.00	0.47	92.4	2152	44
	1.50	0.52	90.0	2111	50
Pure PZT	0.00	0.28	65.0	1580	100

Coulomb–Hartree–Fock formalism [41]. It is termed unrelaxed because the aiPI wavefunctions are not affected by this correction.

The Madelung potential, responsible for the largest part of the interaction energies, has been analytically integrated. Layer-by-layer Ewald summation techniques were used accurately to sum long-range Coulomb potential contributions.

3.3. Model

A schematic representation of the PZT tetragonal structure is depicted in Fig. 1. The PZT structure has been optimized by varying the Ti^{4+}/Zr^{4+} z-fractional coordinate for the rhombohedral (space group *R*3*m*) and tetragonal (space group *P*4*mm*) structures. The remaining structural parameters for pure and doped PZT, lattice and positional parameters, have been kept fixed at their experimental values obtained from X-ray diffraction experiments through using the Rietvel method.

We have defined the polarization parameter (PP) as a measure of lattice stability, related to the variation of lattice energy for tetragonal, ΔE_T, and rhombohedral, ΔE_R, corresponding to a displacement Δz along the *c*-axis from the optimized *z*-value optimized structures

$$\Delta E_S = E_S(\Delta z) - E_{Sopt} \qquad (S = T \text{ or } R) \qquad (5)$$

$$PP = \Delta E_T T(\%) + \Delta E_R R(\%) \qquad (6)$$

$R(\%)$ and $T(\%)$ being the lattice percentage concentration of the rhombohedral and tetrahedral phases, respectively.

4. Results and discussion

The X-ray diffraction pattern of the Ca-PZT samples (Fig. 2), prepared by addition of calcium acetate to ZT and $Pb(OH)_2$ mixtures in isopropyl alcohol followed by calcination at 850 °C and sintering at 1150 °C, shows the diffraction peaks as doublets and triples. The indexing of these peaks as shown in Fig. 2 is consistent with the presence of two phases, one tetragonal (with a higher Ti^{4+} ions content) and one rhombohedral (with a higher Zr^{4+} ions content). The coexistence of these phases can be due to small variations in the composition during the sample preparation. Lal and Krishan [42] do not observe the coexistence of these two ferroelectric phases for materials prepared through the spray-dry process. This can be attributed to the higher chemical homogeneity which restricts composition fluctuations in sintered ceramics.

According to Kakegwa and Mohri [43], the solutions prepared by solid-state reactions yield to the coexistence of the tetragonal and rhombohedral phases for compositions close to the morphotropic phase boundary (MPB) ($0.52 < x < 0.55$) with x being the Zr^{4+}/Ti^{4+} ratio. This coexistence is due to fluctuations in the composition of the Ti^{4+} and Zr^{4+} ions in the PZT structure. Monophasic PZT with compositions close to the MPB composition can be prepared by chemical routes, due to the fact that Ti^{4+} and Zr^{4+} ions are homogeneously distributed in the B^{4+} sites.

In order to avoid the formation of the antiferroelectric $PbZrO_3$ phase, we have prepared the ferroelectric $PbTiO_3$ material. Table I summarizes the synthesis results together with the relative density (ρ/ρ_T) of the various samples (ρ = bulk density and ρ_T = theoretical density). We observe the formation of a unique tetragonal phase for composition close to the MPB region with a low density which disfavours its piezoelectric properties. The calcium doping of

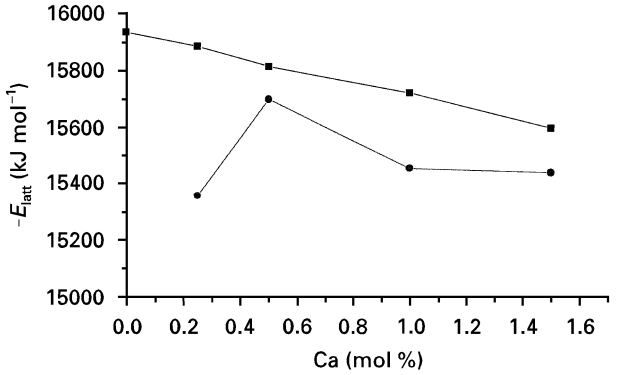

Figure 3 Calculated lattice energy. E_{latt} for both (■) tetragonal and (●) rhombohedral PZT versus the Ca^{2+} concentration.

TABLE II Remanent polarization, P_r, and coercive field, E_c, for pure PZT 53/47 and calcium-doped PZT 53/47

	Dopant (%)	P_r (μC cm^{-3})	E_c (kV/cm^{-1})
Ca-PZT	0.25	8.48	7.60
	0.50	8.65	8.00
	1.00	8.71	10.00
	1.50	9.24	10.00
Pure PZT	0.00	3.15	21.00

PZT 53/47 leads to a shift of the MPB towards the rhombohedral phase. The calcium oxide addition to the PZT 53/47 changes the phase concentration ratio due to the formation of an intermediate phase $CaZrO_3$ which partially modifies the equilibrium towards the formation of the rhombohedral phase. This effect had already been observed [13], and we do not appreciate any substantial change regarding phase ratio (rhombohedral/tetrahedral) for the calcium-doped samples.

Calculations of lattice energy for both structures using the aiPI method show that an increase in the Ca^{2+} concentration produces a decrease in the stability of the tetragonal structure while the rhombohedral phase is stabilized until the concentration of 0.5 mol % for calcium is achieved (see Fig. 3).

From a structural point of view, the addition of Ca^{2+} to the PZT causes a decrease of the tetrahedral cell parameter, a_t, and an increase of the c_t tetrahedral cell parameter. Consequently, one would expect higher dipolar moments, when electromechanically stretched, for the Ca-PZT 53/47 structure with a $(c/a)_t$ ratio of 1.033 than for the Ca-PZT with a $(c/a)_t$ ratio of 1.022. These variations in cell parameters can be due to a stronger repulsion of the Ca^{2+} cations with the Zr^{4+} and Ti^{4+} ions, which causes a more compact packing of the structure. The rhombohedral cell parameters change very little, $a_r = 407.1$ pm and $\alpha = 89.75^\circ$ when the doping agent is added.

The remanent polarization, P_r, and the coercive field of the materials reported in this work are presented in Table II. We observe an increase in the remanent polarization and the coercive field of the Ca-PZT 53/57 when the dopant concentration is increased. The higher P_r values are obtained for calcium molar concentrations of 1.5%. This implies important

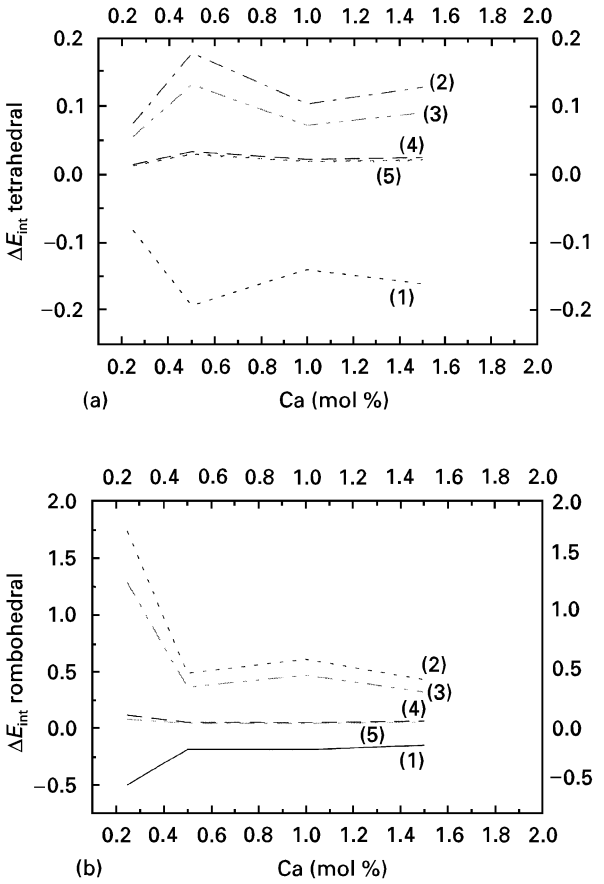

Figure 4 Variation of ion-lattice interaction energy, E_{int}, for each of the ions in the lattice as a function of the Ca^{2+} concentration for the (a) tetrahedral and (b) rhombohedral phases (1) O^{2-}, (2) Zr^{4+}, (3) Ti^{4+}, (4) Pb^{2+}, (5) Ba^{21}.

changes in the electrical properties of the material when CaO is added. The remanent polarization values for the calcium-doped PZT 53/57 samples are higher than those of the undoped PZT 53/57 while the opposite trend has been observed for the coercive field measurements. The addition of calcium to $PbZrO_3$ causes an increase in the antiferroelectric character [26]. However, this phase can be redirectioned by strong electric fields ($\geqslant 3$ kV mm^{-1}) which results in no increase of the remanent polarization.

Fig. 4 represents the ion–lattice interaction energy, E_{int}, for each of the ions in the lattice as a function of the Ca^{2+} concentration for the tetrahedral and rhombohedral phases. An increase on the Ca^{2+} concentration produces an opposite trend in these two phases. The lower repulsion has been calculated for 0.25% calcium concentration for the rhombohedral structure.

Fig. 5 shows a representation of the polarization parameter versus the molar calcium concentration (%). The PZT, calcium doping increases in a significant way the remanent polarization and the theoretical results represented in Fig. 5 indicate this effect. An increase of the doping agent concentration produces a higher polarization degree, favouring the remanent polarization.

The lower coercive field, E_c, values of the calcium-doped PZT 53/47 can be attributed to the higher vibrational frequencies of the doped structure which

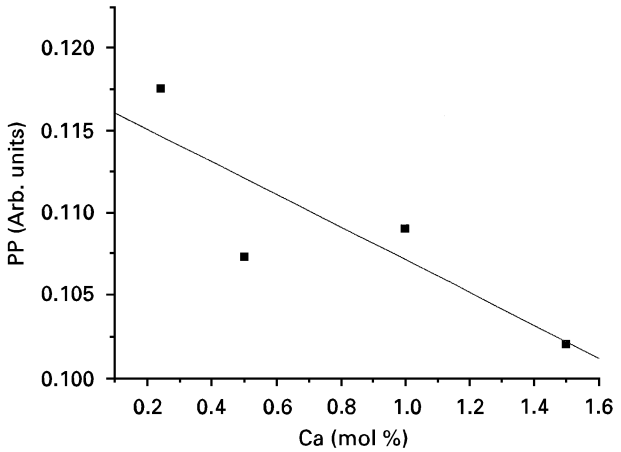

Figure 5 Representation of the polarization parameter, PP, versus the molar calcium concentration.

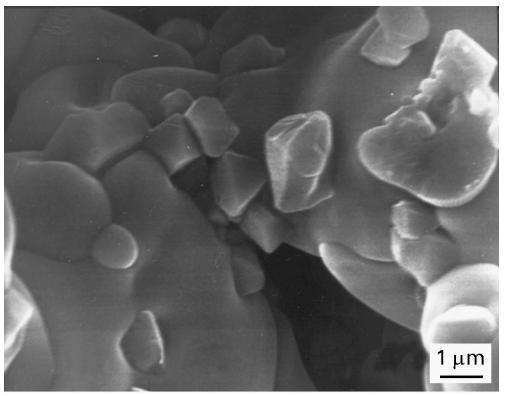

Figure 6 The pure PZT 53/47 sample microstructure.

results in lower energy requirement for dipole inversion [44].

Table I lists the planar coupling factors, K_p, and frequency-thickness constants, N_p, for the pure and doped structures. The K_p and N_p values, as well as the densities, are higher for the doped structures. The K_p measurements are the results of a bulk effect.

The coercive field can be related with the stretching of the oxygen–metal bond in the structure. In that sense, the PZT transductor effect or reverse effect can be attributed to the interplanar displacement under electrical stretching.

The planar coupling factor changes very little with the dopant concentration. This result agrees with an increase in the remanent polarization and coercive field. However, K_p is very small for undoped PZT.

We observe an imbalance between the polarization effect in regard to the coercive field because the transductor effect or reverse effect energy requirements increase when the calcium concentration is increased.

The K_p values are independent of the density of the samples and, as a consequence, K_p depends only on the network or lattice.

Kulcsar *et al.* [22] have studied calcium doped PZT structures prepared from the oxides mixture and have reported K_p and density values of 0.44 and 7.26 $g\,cm^{-3}$, respectively. Both measurements are close to the ones reported in this work.

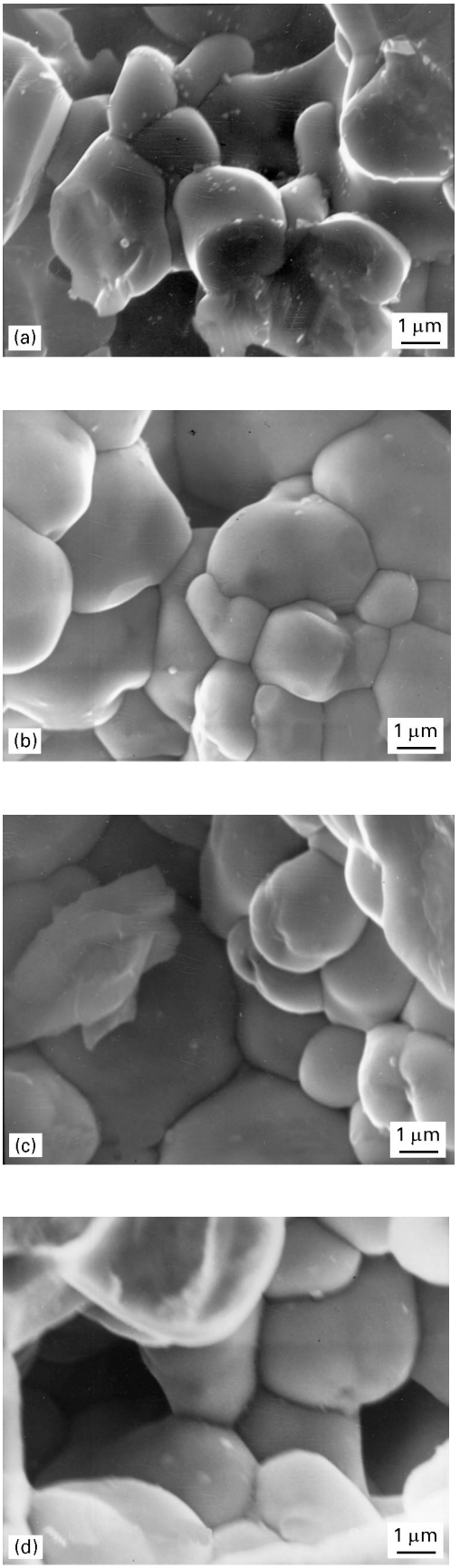

Figure 7 The Ca-PZT 53/47 doped samples microstructure. Calcium molar concentration: (a) 0.25%, (b) 0.50%, (c) 1.00% and (d) 1.50%.

The wave propagation on the material depends on the structure. Frequency–thickness constant values increase when the density increases. This fact shows that there is a direct relationship between the wave

propagation speed in the material and its microstructure.

The calcium-doped PZT microstructures show that calcium addition improves the densification. The pure PZT microstructure (Fig. 6) shows a broad particle grain-size distribution while the calcium-doped PZT microstructure (Fig. 7) presents a more homogeneous distribution (between 1.5 and 4.0 μm). These data confirm our electrical measurements results for pure and calcium-doped PZT 53/47 structures in the sense that higher K_p, N_p and density values are obtained for the doped structures.

5. Conclusion

The remanent polarization increases with calcium concentration due to the polarization of the unit cell promoted by the calcium ion. Both the planar coupling factor and the frequency–thickness constant increase with calcium concentration in relation to pure PZT, mainly due to an increase in relative density.

The lattice energy decreases with calcium addition on both tetragonal and rhombohedral phases, as determined theoretically.

Acknowledgements

Financial support from the research funds of PADCT/FINEP and CNPq is gratefully acknowledged. We thank Dr Carlos Paiva-Santos for the analysis of X-ray data, and Victor Luaña for sending us the latest version of the aiPI method.

References

1. T. KAWAGUCHI, H. ADACHI, K. SETSUNE, O. YAMAZAKI and K. WASA, *Appl. Opt.* **23** (1984) 2187.
2. A. KUMADA, *Jpn. J. Appl. Phys.* **24** (1985) 739.
3. K. UCHINO, *Bull. Am. Ceram. Soc.* **65** (1986) 647.
4. V. E. WOOD, J. R. BUSCH, S. D. RAMAMURTHI and S. L. SWARTZ, *J. Appl. Phys.* **71** (1992) 4557.
5. K. D. PRESTON and G. H. HAERTLING, *Appl. Phys. Lett.* **60** (1992) 2831.
6. C. C. HSUEH, T. TAMAGAWA, A. HELGELSON and D. L. POLLA, *Integr. Ferroelect.* **3** (1993) 21.
7. V. I. PETROVSKY, A. S. SIGOV and K. A. VOROTILOV, *ibid.* **3** (1993) 59.
8. E. M. LINES and A. M. GLASS, "Principles and Applications of Ferroelectrics and Related Materials" (Claredon, Oxford, 1977).
9. B. JAFFE, W. R. COOK and H. JAFFE, "Piezoelectric Ceramics" (Academic, New York, 1971)
10. S. NOMURA and S. SAWADA, *J. Phys. Soc. Jpn* **10** (1955) 108.
11. O. YAMAGUCHI and H. MOGI, *J. Am. Ceram. Soc.* **72** (1989) 1065.
12. T. YAMAMOTO, *Am. Ceram. Soc. Bull.* **71** (1992) 978.
13. S. K. SAHA and D. AGRAWAL, *ibid.* **71** (1992) 1424.
14. S. STOTZ, *Ferroelectrics* **76** (1987) 123.
15. A. V. TURIK, M. F. KUPRIYANOV, E. N. SIDORENKO and S. M. ZAITSEV, *Sov. Phys. Tech. Phys.* **25** (1987) 1251.
16. B. V. HIMERATH, A. I KINGON and J. V. BIGGERS, *J. Am. Ceram. Soc.* **66** (1983) 790.
17. T. OHMO, M. TAKAHASHI and N. TSUBOUCHI, *J. Jpn Soc. Powder Metall.* **20** (1973) 154.
18. T. YAMAGUCHI, S. H. CHO, M. MAKAMORI and H. KUNO, *Ceram. Int.* **2** (1976) 76.
19. S. VENKATARAMANI and J. V. BIGGERS, *Am. Ceram. Soc. Bull.* **59** (1980) 462.
20. Y. MATSUO and H. SASAKI, *J. Am. Ceram. Soc.* **48** (1965) 289.
21. D. L. HANKEY, PhD thesis, Pennsylvania State University (1980).
22. F. KULCSAR, *J. Am. Ceram. Soc.* **42** (1959) 49.
23. J. BERNARD, "Piezoelectric Ceramics" (Academic, London, 1971).
24. Q. M. ZHANG, H. WANG, N. KIM and L. E. CROSS, *J. Appl. Phys.* **1** (1994) 75.
25. F. VASILIU, G. LUCUTA and F. CONSTANTINESCU, *Phys. Status Solidi* **80** (1983) 637.
26. G. SHIRANE and K. SUZUKI, *J. Phys. Soc. Jpn* **8** (1953) 615.
27. R. COMES, M. LAMBERT and A. GUINIER, *Acta Crystallogr.* **A26** (1970) 244.
28. V. LUAÑA and L. PUEYO, *J. Mol. Struct.* (*THEOCHEM*) **166** (1988) 215.
29. V. LUAÑA, F. RECIO and L. PUEYO, *Phys. Rev. B* **42** (1990) 1791.
30. M. FLÓREZ, E. FRANCISCO, V. LUAÑA, A. MARTÍN-PENDÁS, J. M. RECIO, M. BERMEJO and L. PUEYO, in "Cluster Models for Surface and Bulk Phemomena", edited by G. Pacchioni, P. S. Bagus and F. Parmigiani (Plenum Press, New York, 1992) p. 605.
31. V. LUAÑA and L. PUEYO, *Phys. Rev. B* 41 (1990) 3800.
32. V. LUAÑA, M. FLOREZ, E. FRANCISCO, A. MARTIN-PENDÁS, J. M. RECIO, M. BERMEJO and L. PUEYO, in "Cluster Models for Surface and Bulk Phemomena", edited by G. Pacchioni, P. S. Bagus and F. Parmigiani (Plenum Press, New York, 1992) p. 619.
33. A. BELTRÁN, A. FLORES-RIVEROS, J. A. IGUALADA, G. MONRÓS, J. ANDRÉS, V. LUAÑA and A. MARTÍN-PENDÁS, *J. Phys. Chem.* **97** (1993) 2555.
34. J. ANDRÉS, A. BELTRÁN, J. CARDA and G. MONRÓS, *Int. J. Quantum. Chem. Symp.* **27** (1993) 175.
35. J. ANDRÉS and A. BELTRÁN, *Chem. Phys. Lett.* **221** (1994) 249.
36. C.P. PAIVA-SANTOS, Ph. thesis, IFQSc-USP (1990).
37. S. HUZINAGA and A. A. CANTU, *J. Chem. Phys.* **55** (1971) 5543.
38. V. LUAÑA and L. PUEYO, *Phys. Rev. B* **39** (1989) 11093.
39. E. CLEMENTI and C. ROETTI, *At. Data Nucl. Data Tables* **14** (1974) 177.
40. A. D. McLEAN and R. S. McLEAN, *ibid.* **26** (1981) 197.
41. S. J. CHAKRAVORTY and E. CLEMENTI, *Phys. Rev. A* **39** (1989) 2290.
42. R. LAL and R. KRISHAN, *Br. Ceram. Trans. J* **87** (1988) 99.
43. K. KAKEGAWA and J. A. MOHRI, *Solid State Commun.* **64** (1977) 769.
44. H. BANNO and T. TSUNOOKA, *Jpn. J. Appl. Phys.* **6** (1967) 954.

Received 23 February
and accepted 3 October 1996